Published in final edited form as:
J Phys Chem Lett. 2013 June 6; 4(11): 1866–1871. doi:10.1021/jz400826a.

Quantum Beats and Coherence Decay in Degenerate States Split by Solvation

Lev Chuntonov[*], **Daniel G. Kuroda**, **Ayanjeet Ghosh**, **Jianqiang Ma**, and **Robin M. Hochstrasser**[a]
Ultrafast Optical Processes Laboratory, Department of Chemistry, University of Pennsylvania, Philadelphia PA, 19104, USA

Abstract

Coherent dynamics of degenerate quantum states symmetry-broken on the femtosecond timescale is found to exhibit the phenomenon of quantum beats. Frequency-resolved and polarization-selective heterodyned transient grating spectroscopy enabled us to retrieve the oscillation pattern characteristic of the beating in systems undergoing ultrafast dynamical processes. This methodology applies to the general phenomena of coherence dynamics which is important in any ultrafast multidimensional spectroscopy. A particular application to the vibrational spectroscopy of coherence in the degenerate normal modes of the tricyanomethanide anion solvated in water is explored in this study. The relaxation of the cross-polarization transient grating anisotropy is shown to reflect the loss of the vibrational coherence, which is caused by ultrafast dynamics of the water solvation shell.

Keywords

quantum beats; solvation dynamics; vibrational coherence relaxation; anisotropy; frequency-resolved transient grating; tricyanomethanide ion

The study of quantum coherence and its relaxation in condensed phase has been made possible by means of ultrafast multipulse spectroscopy.[1–5] Quantum coherence is of fundamental interest for studies of the mechanisms by which excited states lose correlation[6–8] or transfer coherence from one pair of states to another.[5,9–13] It was also found to play an important role in the biological systems.[5,14,15] Interpretation of structural and dynamical information obtained from experiments involving coherent excitations requires detailed understanding of all the relaxation processes.[1,9,16] In the field of vibrational spectroscopy experimental advances in ultrafast multidimensional methods have demonstrated how the study of relaxation dynamics can elucidate some important aspects of the interaction between a molecule and its environment.[17–23] Recent examples include the solvation dynamics in bulk and at the interfaces,[19,21,23–25] chemical exchange,[26–28] conformational dynamics,[29,30] and binding processes in proteins and drugs.[31–33]

Identification of relaxation mechanisms and their time scales is an important step towards characterization of the system dynamics in solution. Full- and near-degeneracy of quantum state structure is a common scenario especially in the vibrational modes of highly symmetric molecules.[24,34–39] In the present work we report the direct observation of the coherence

[*]Corresponding author, chuntl@sas.upenn.edu, phone: 215-898-8247, fax: 215-898-0590.
[a]Author Status: Professor Robin M. Hochstrasser passed away on February 27, 2013.

Supporting Information Available: Derivation of equation (3) and additional experimental data. This material is available free of charge via the Internet at http://pubs.acs.org.

dynamics of tricyanomethanide anion (TCM) in water. TCM has become the focus of extensive research due to its possible application in ionic liquids.[40] TCM has three nitrile groups connected to the central carbon atom and in the absence of the interaction with the environment it has D_{3h} symmetry. Two degenerate in-plane normal vibrational modes referred to as A_1 and A_2 corresponding to asymmetric stretching appear as a single peak at 2173 cm^{-1} in the linear infrared absorption spectrum.[41,42] In aqueous solution the interaction between the TCM and water molecules dynamically breaks the three-fold rotational symmetry of the anion and lifts the degeneracy of the in-plane modes. Heterodyned three-pulse photon echo spectroscopy has a unique ability to resolve the femtosecond dynamics of the coupled quantum states of the solvated molecules.[43–45] In a recent study, the average splitting of 7 cm^{-1} between the A_1 and A_2 modes of TCM was revealed by 2DIR spectroscopy.[36] Here we demonstrate that even in the presence of ultrafast fluctuation of the solvation shell, which induces frequency fluctuations and mixing of the nearly degenerate vibrational modes, the signature of the coherence in the symmetry-broken molecules can be monitored as a beating pattern and characterized with polarization-selective and frequency-resolved heterodyned transient grating (FRHTG) infrared spectroscopy. We anticipate that the concept demonstrated here can be generally applied to a broad range of problems studied by ultrafast multidimensional spectroscopy.[1–3]

Until now vibrational coherence dynamics was studied in systems where the quantum states have strong transition dipole moments and strong coupling which results in a high signal-to-noise ratio and high spectral separation.[10–12] In many other interesting systems as, for example, proteins studied by isotope labeling or molecules with high symmetry, which involve weak and overlapping transitions,[21–23,37] coherence dynamics is not easily observed. In such scenarios polarization-resolved spectroscopy has been demonstrated to be particularly useful, allowing one to isolate otherwise hidden signals.[46] Due to the degeneracy of the vibrational modes in TCM, the quantum beats cannot be observed by ultrafast IR pump-probe spectroscopy or standard 2DIR spectroscopy[10,11] because the spectral overlap between the beating and not-beating Liouville pathways[2,3] masks the beating pattern.

In a FRHTG experiment, schematically shown in Figure 1a, the signal is a sum of all the relevant Liouville pathways[47] which track the system's evolution during the interaction with femtosecond pulses (see Figure 1b–e). Coherent states are prepared by interaction with the first pulse pair, evolve during the waiting time (T), and are measured by the second pair of pulses during the detection time (t). The signal represents an average over the isotropic molecular dipoles distribution.

Consider the coherent excitation of two coupled vibrational modes. Assuming that the excitation femtosecond pulses are infinitely short, the FRHTG signal $S^{\mathrm{ABCD}}(\omega,\mathrm{T})$ collected with the sequence of pulses linearly polarized along the directions A,B,C,D in the laboratory frame is proportional to the Fourier transform over all contributing response functions[2,3] $R_n(\mathrm{T}, t)$:

$$S^{\mathrm{ABCD}}(\omega,\mathrm{T}) \propto i\sum_n \langle i_{\mathrm{A}} j_{\mathrm{B}} k_{\mathrm{C}} l_{\mathrm{D}}\rangle \int_0^\infty R_n(\mathrm{T},t)e^{i\omega t}dt = \sum_n \langle i_{\mathrm{A}} j_{\mathrm{B}} k_{\mathrm{C}} l_{\mathrm{D}}\rangle S_{ijkl}(\omega,\mathrm{T}), \quad (1)$$

where $\langle i_{\mathrm{A}}\, j_{\mathrm{B}}\, k_{\mathrm{C}}\, l_{\mathrm{D}}\rangle$ represents ensemble-averaged rotational factor of the Feynman path i,j,k,l (enumerated by index n), and $S_{ijkl}(\omega,\mathrm{T})$ are the corresponding spectral amplitudes. The real part of $S^{\mathrm{XXXX}}(\omega)$ for the TCM anion is shown in FIGURE 2. The splitting between the A_1 and A_2 modes is not sufficient to resolve the two peaks, thus, only a single peak is seen in the FRHTG spectrum. Similar to the standard frequency-resolved pump-

probe signal, the negative and positive peaks at 2152 and 2173 cm^{-1} correspond to the transient absorption and stimulated emission and ground state bleach signals, respectively.[36] For completeness, Figure 2 also presents the linear absorption spectrum of TCM in water (panels a–b).

The Liouville pathways for the transient grating experiment are shown in Figure 1b–e. The population states $|i\rangle\langle i|$ that appear in diagrams of panels b–c do not show beating oscillations during the waiting time, while the coherence states $|i\rangle\langle i|$ (panels d–e) do beat. As already mentioned, due to the masking effect by the non-beating Liouville pathways beating is not observed during the waiting time in the $S^{XXXX}(\omega, T)$ signal. Therefore, in order to resolve the beating pattern we first examine the waiting time dependence of the parallel-polarization transient grating (PPTG) anisotropy. The PPTG anisotropy signal $r_{PPTG}(\omega, T)$ is calculated from two waiting time scans, where the system is prepared by the first two pulses having the same polarization and the evolution is probed by the pair of pulses polarized either parallel or perpendicular to the initial pulse pair:[29]

$$r_{PPTG}(\omega, T)=\frac{S^{XXXX}(\omega, T) - S^{YYXX}(\omega, T)}{S^{XXXX}(\omega, T)+2S^{YYXX}(\omega, T)}$$

. A discussion on the pump-probe anisotropy, which at T=0 is formally equivalent to $r_{PPTG}(\omega, T=0)$ was recently published.[37] Here we note that in PPTG anisotropy signal the vibrational population relaxation factor $e^{-T/2T_1}$ is canceled out, and when a simplified model of PPTG anisotropy is considered,[48] the expected relaxation by the rotational diffusion is $r_{PPTG}(T) \propto e^{-6DT}$, where D is the rotational diffusion constant. The waiting time dependence of S^{XXXX} and S^{YYXX} signals at 2173 cm^{-1} are shown in Figure S1 of the Supporting Information.

The PPTG anisotropy signal at 2173 cm^{-1} in Figure 2e shows a bi-exponential decay with slow (τ =2.4 ± 1.4 ps) and fast (τ =0.5 ± 0.1 ps) components, attributed to the rotational diffusion relaxation and mode mixing, respectively, in a full agreement with previously published pump-probe results.[36] While appearance of a beating pattern due to the excitation of the coherence states is expected in the PPTG anisotropy, from numerical simulations described below we find that it occurs for strong and well spectrally-separated modes, or if one of the transition dipole moments is significantly stronger than the other. Clearly, this is not the case for the TCM anion. The A_1 and A_2 vibrational modes are nearly degenerate and have transition dipole moments of the same magnitude, which results in a spectral overlap between the beating and not-beating pathways contributing to the signal. In the PPTG anisotropy signal in Figure 2e, the oscillatory behavior is masked completely, while the appearance of a fast decaying component suggests the presence of a population mixing mechanism in addition to rotational diffusion.

To validate our interpretation of the experimental results, we used numerical simulations based on the third order response functions[1–3] applied to two coupled vibrational modes. For all model parameters we have used experimentally measured values[36] listed in Table 1, with the exception of amplitude $\Delta\omega$ for the frequency fluctuation correlation function $\xi(t)$, which is not readily available from our experimental data. This parameter was selected to provide the best match to the experimental results. We have used Kubo correlation function[2] $\xi_{ij}(t) = \Delta\omega^2 e^{-t/\tau_C}$ (τ_C is the correlation time) for both auto-correlation (ξ_{ii}) and cross-correlation (ξ_{ij}), such that $\xi_{ij} = f\,\xi_{ii}$, where f is the correlation coefficient, which was found to correctly describe dynamics of TCM in water.[36] In simulations we included also the population and coherence transfer using the methodology based on Redfield's theory that was established previously.[10,34,35,38] The simulation results are in a good agreement with the experiment, as shown in Figures 2b,d,f.

Thus, the beating pattern indicating coherence between the two nearly degenerate modes of the TCM cannot be observed in PPTG anisotropy. We therefore used different pulse-

polarization conditions to reveal the coherence dynamics. Anisotropic response of the molecules allows one to extract only those Liouville pathways that contain the information on the coupled modes coherent dynamics during the waiting time (i.e. beating pathways shown in Figure 1d–e) and to eliminate all the others. The excited states were prepared with a pair of cross-polarized pulses and probed with two sets of pulses having different cross-polarization. The measured signal is the cross-polarization transient grating (CPTG) anisotropy $r_{\mathrm{CPTG}}(\omega, \mathrm{T})$that is the difference between the signals corresponding to polarization conditions $\langle \mathrm{XYYX} \rangle$ and $\langle \mathrm{YXYX} \rangle$: $r_{\mathrm{CPTG}}(\omega, \mathrm{T}) = S^{\mathrm{XYYX}}(\omega, \mathrm{T}) - S^{\mathrm{YXYX}}(\omega, \mathrm{T})$. It can be readily shown that as opposed to PPTG anisotropy, in CPTG anisotropy most of the Liouville pathways are eliminated by subtraction,[46,48] and the remaining Liouville pathways only involve the excitation and waiting time evolution of the coherence states $|i\rangle\langle j|$. The waiting time dependence of S^{XYYX} and S^{YXYX} at 2173 cm^{-1} are shown in Figure S1 of the Supporting Information.

Experimental results for the waiting time dependence of the CPTG anisotropy signal at 2173 cm^{-1} are shown in Figure 3a, where the beating pattern is clearly seen. The relatively fast decay of the oscillations appears on the same time scale as the fast decay component observed in the PPTG anisotropy in Figure 2. However, as will be shown below it has a different origin.

We analyze the CPTGA results by expressing the signal as

$$r_{\mathrm{CPTG}}(\omega, \mathrm{T}) = \sum_{n} (\langle i_{\mathrm{X}} j_{\mathrm{Y}} k_{\mathrm{Y}} l_{\mathrm{X}} \rangle - \langle i_{\mathrm{X}} j_{\mathrm{Y}} k_{\mathrm{X}} l_{\mathrm{Y}} \rangle) S_{ijkl}(\omega, \mathrm{T}). \quad (2)$$

When the relevant Liouville pathways and their rotational factors are explicitly introduced, CPTG anisotropy takes the form of (see Supporting Information)

$$r_{\mathrm{CPTG}}(\omega, \mathrm{T}) = \mu_1^2 \mu_2^2 e^{-g(\mathrm{T})} e^{-2D\mathrm{T}} e^{-\mathrm{T}/T_1} \cos(\omega_{12}\mathrm{T}) \sum_{i=1}^{2} S_i(\omega - \omega_i, \mathrm{T}) - S_i(\omega - \omega_i - \delta, \mathrm{T}), \quad (3)$$

where $\mu_1 = \mu_2$ are the transition dipole moments associated with the vibrational modes, ω_{12} is the difference in their fundamental transition frequencies, and δ is the combination band anharmonicity. The waiting time dependence of the spectral lineshapes $S_i(\omega, \mathrm{T})$arises from the dependence of the response functions on the lineshape function $g(\mathrm{T} + t)$, which is a double integral of ξ. Generally, the dependence of $g(\mathrm{T} + t)$ on the waiting and detection time intervals cannot be separated. However in the homogeneous limit, the two time intervals become separable and the spectral shapes are Lorentzian and stationary during the waiting time. In the inhomogeneous limit the spectral shapes are Voigt functions, i.e. a convolution of Lorentzian and Gaussian functions,[47] where the Lorentzian component gradually changes during the waiting time. Although for the TCM anion we used Kubo lineshapes and the spectral amplitudes $S_i(\omega,\mathrm{T})$ have some waiting time dependence, as we will show below, the model in equation(3) can be further simplified by assuming that this effect is minor as compared to the oscillating and decaying components.

The waiting time dependence of the CPTG anisotropy differs from PPTG anisotropy in that it decays both due to the lifetime T_1 and rotational diffusion, such that the total decay of the vibrational coherence measured in CPTG anisotropy is due to the factor $e^{-g(\mathrm{T})-2D\mathrm{T}-\mathrm{T}/T_1}$. As both rotational diffusion and the population relaxation times in the TCM anion are slow (see Table 1), the coherence relaxation decay is dominated by the factor $e^{-g(\mathrm{T})}$. Fitting the experimental data in Figure 3a to the function of equation (3) results in a coherence decay time of τ =450 ± 10 fs. The correlation time of TCM anion τ_C =1.1 ps associated with the decay of the correlation function ξ (T) was measured previously.[36] In the case of a Kubo

lineshape the relation between the decay constants of ξ (T) and $e^{-g(T)}$ does not have a simple mathematical expression. Thus, we resort to a numerical simulation of the experiments. The simulation results shown in Figure 3b in blue line support our observation that the coherence decay arise primarily from the correlation time of ξ (T) , with additional contribution as appear in equation (3) that results in a difference between τ =450 fs and τ =1.1 ps decay constants. We have found a good agreement between the experimental and simulated results using only a single correlation time constant τ_C for ξ (T) , which successfully reproduces the decays in both ξ (T) and in CPTG anisotropy. These results suggest that the coherence relaxation is caused primarily by the fluctuation of the solvation shell with additional contributions from rotational diffusion and vibrational lifetime.

Until now we have neglected the processes of population or coherence transfer in the CPTG anisotropy model (equation (3)). These two processes are known to contribute to the vibrational dynamics of TCM.[36] Below, we will demonstrate that a quantitative description requires detailed accounting for these processes, by their incorporation into the simulations. Based on the recent studies[10,11,34–36,38] it is reasonable to assume here that events of population and coherence transfer occur mainly during the waiting time, and that the transfer rate constants between the population and coherence states as well as between coherences involving ground and excited states are negligible. Also due to the near-degeneracy of the normal modes, remaining transfer rate constants between the population states $|i\rangle\langle i|$ and $|j\rangle\langle j|$ as well as between coherences $|i\rangle\langle j|$ and $|j\rangle\langle i|$ are assumed to have the same value k_{et}. When the transfer processes are accounted for, better agreement with the experimental results is observed (black line in Figure 3b). Due to the significant complication that a full theoretical description implies,[49] we have not included these processes in equation (3), yet keeping our model valid qualitatively. The model that includes the transfer processes will be addressed in a future work. However, the small difference in the decay time of the blue and black lines in Figure 3b (ca. 650 fs vs 500 fs) suggests again that the main contribution to the coherence relaxation observed here is due to the frequency fluctuation caused by the hydration dynamics and only a minor contribution is due to the population transfer.

The effect of the hydration dynamics is further emphasized when the solvent is changed from water to the aprotic dimethyl sulfoxide. In this case of weak solute-solvent interaction, the width of the nitrile linear infrared absorption peak corresponding to the A_1 and A_2 vibrational modes of TCM changes[42] from 17 to 10 cm^{-1}. Due to the different character of interaction with the solvent, the symmetry breaking is less pronounced and splitting of the degenerate modes is as small as ca. 2 cm^{-1}. In this case CPTG anisotropy measures coherence relaxation time of 1 ps (note that vibrational lifetime is ca. 40 ps)[42], as shown in Figure S2 of Supporting Information.

In conclusion, we have presented a methodology to directly characterize the ultrafast dynamics of coherence in the nearly-degenerate quantum states. A proper choice of the polarization conditions of ultrafast pulses enabled us to eliminate all the excitation pathways that mask the quantum beat pattern. In particular, we have applied this methodology to investigate the coherent dynamics of the nearly degenerate vibrational normal modes of the TCM anion in water. Our experimental results and their modeling show that the relaxation of the cross-polarization transient grating anisotropy is due to the loss of the vibrational coherence, which is caused principally by the solvation dynamics and is manifested through the lineshape function. These results are significant for studies of fundamental processes as, for example, coherence transfer, and for development of new approaches to study structural dynamics in biomolecules. We anticipate that the novel approach is generally applicable to a broad range of systems with fully- or nearly-degenerate quantum states, studied by means of ultrafast multidimensional spectroscopy.

EXPERIMENTAL METHODS

The FRHTG experiment was carried with four linearly-polarized ca. 75 fs mid-IR pulses focused in the BOXCARS geometry. Polarization was rotated by true zero-order waveplates. High-extinction wire-grid polarizers (Specac Ltd., extinction ratio ca. 1:700) were placed right before the focusing lens to avoid depolarization upon reflections. Additional polarizer on the signal beam was placed immediately after the sample cell. The heterodyne pulse preceding the excitation pulses by 1 ps was overlapped with the signal dispersed onto the liquid nitrogen-cooled array detector coupled to the spectrograph.

A solution of 0.1 M of potassium tricyanomethanide (99%, Alfa Aesar) in water and dimethyl sulfoxide was placed between CaF_2 windows with 6 micron spacer. In all experiments the optical density of the sample was kept below 0.2.

Supplementary Material

Refer to Web version on PubMed Central for supplementary material.

Acknowledgments

This research was supported by Grants NIH-GM12592 and P41GM104605 to R.M.H.

REFERENCES

1. Mukamel, S. Principles of Nonlinear Optical Spectroscopy. New York: Oxford University Press; 1995.
2. Hamm, P.; Zanni, MT. Concepts and Methods of 2D Infrared Spectroscopy. Cambridge: Cambridge University Press; 2011.
3. Cho, M. Two-Dimensional Optical Spectroscopy. Boca Raton: Taylor & Francis; 2010.
4. Jonas DM. Two-Dimensional Femtosecond Spectroscopy. Ann. Rev. Phys. Chem. 2003; 54:425–463. [PubMed: 12626736]
5. Fleming G, Huelga S, Plenio M. Focus on Quantum Effects and Noise in Biomolecules. New J. Phys. 2011; 13:115002.
6. Hamm P, Lim M, Hochstrasser RM. Vibrational Energy Relaxation of the Cyanide Ion in Water. J. Chem. Phys. 1997; 107:10523–10531.
7. Asbury JB, Steinel T, Stromberg C, Corcelli SA, Lawrence CP, Skinner JL, Fayer MD. Water Dynamics: Vibrational Echo Correlation Spectroscopy and Comparison to Molecular Dynamics Simulations. J. Phys. Chem. A. 2004; 108:1107–1119.
8. Demirdöven N, Khalil M, Tokmakoff A. Correlated Vibrational Dynamics Revealed by Two-Dimensional. Infrared Spectroscopy. 2002; 89:237401.
9. Piryatinski A, Chernyak V, Mukamel S. Vibrational-Exciton Relaxation Probed by Three-Pulse Echoes in Polypeptides. Chem. Phys. 2001; 266:285–294.
10. Khalil M, Demirdoven N, Tokmakoff A. Vibrational Coherence Transfer Characterized with Fourier-Transform 2d Ir Spectroscopy. J. Chem. Phys. 2004; 121:362–373. [PubMed: 15260555]
11. Nee MJ, Baiz CR, Anna JM, McCanne R, Kubarych KJ. Multilevel Vibrational Coherence Transfer and Wavepacket Dynamics Probed with Multidimensional IR Spectroscopy. J. Chem. Phys. 2008; 129:084503–084511. [PubMed: 19044831]
12. Pakoulev AV, Rickard MA, Mathew NA, Kornau KM, Wright JC. Frequency-Domain Time-Resolved Four Wave Mixing Spectroscopy of Vibrational Coherence Transfer with Single-Color Excitation. J. Phys. Chem. A. 2008; 112:6320–6329. [PubMed: 18572931]
13. Collini E, Scholes GD. Coherent Intrachain Energy Migration in a Conjugated Polymer at Room Temperature. Science. 2009; 323:369–373. [PubMed: 19150843]
14. Fidler AF, Caram JR, Hayes D, Engel GS. Towards a Coherent Picture of Excitonic Coherence in the Fenna–Matthews–Olson Complex. J. Phys. B. 2012; 45:154013.

15. Scholes GD. Quantum-Coherent Electronic Energy Transfer: Did Nature Think of It First? J. Phys. Chem. Lett. 2010; 1:2–8.
16. Mukamel S. Multidimensional Femtosecond Correlation Spectroscopies of Electronic and Vibrational Excitations. Ann. Rev. Phys. Chem. 2000; 51:691–729. [PubMed: 11031297]
17. Hamm P, Lim M, Hochstrasser RM. Structure of the Amide I Band of Peptides Measured by Femtosecond Nonlinear-Infrared Spectroscopy. J. Phys. Chem. B. 1998; 102:6123–6138.
18. Hamm P, Lim M, DeGrado WF, Hochstrasser RM. The Two-Dimensional IR Nonlinear Spectroscopy of a Cyclic Penta-Peptide in Relation to Its Three-Dimensional Structure. Proc. Nat. Acad. Sci. 1999; 96:2036–2041. [PubMed: 10051590]
19. Kim YS, Hochstrasser RM. Applications of 2D IR Spectroscopy to Peptides, Proteins, and Hydrogen-Bond Dynamics. J. Phys. Chem. B. 2009; 113:8231–8251. [PubMed: 19351162]
20. Rubtsov IV. Relaxation-Assisted Two-Dimensional Infrared (RA 2D IR) Method: Accessing Distances over 10 Å and Measuring Bond Connectivity Patterns. Acc. Chem. Res. 2009; 42:1385–1394. [PubMed: 19462972]
21. Ghosh A, Qiu J, DeGrado WF, Hochstrasser RM. Tidal Surge in the M2 Proton Channel, Sensed by 2D IR Spectroscopy. Proc. Nat. Acad. Sci. 2011; 108:6115–6120. [PubMed: 21444789]
22. Remorino A, Hochstrasser RM. Three-Dimensional Structures by Two-Dimensional Vibrational Spectroscopy. Acc. Chem. Res. 2012; 45:1896–1905. [PubMed: 22458539]
23. Kim YS, Liu L, Axelsen PH, Hochstrasser RM. 2D IR Provides Evidence for Mobile Water Molecules in b-Amyloid Fibrils. Proc. Nat. Acad. Sci. 2009; 106:17751–17756. [PubMed: 19815514]
24. Thøgersen J, Réhault J, Odelius M, Ogden T, Jena NK, Jensen SJK, Keiding SR, Helbing J. Hydration Dynamics of Aqueous Nitrate. J. Phys. Chem. B. 2013; 117:3376–3388. [PubMed: 23461818]
25. Costard R, Greve C, Heisler IA, Elsaesser T. Ultrafast Energy Redistribution in Local Hydration Shells of Phospholipids: A Two-Dimensional Infrared Study. J. Phys. Chem. Lett. 2012; 3:3646–3651.
26. Zheng J, Kwak K, Asbury J, Chen X, Piletic IR, Fayer MD. Ultrafast Dynamics of Solute-Solvent Complexation Observed at Thermal Equilibrium in Real Time. Science. 2005; 309:1338–1343. [PubMed: 16081697]
27. Kim YS, Hochstrasser RM. Chemical Exchange 2D IR of Hydrogen-Bond Making and Breaking. Proc. Nat. Acad. Sci. 2005; 102:11185–11190. [PubMed: 16040800]
28. Ghosh A, Remorino A, Tucker MJ, Hochstrasser RM. 2D IR Photon Echo Spectroscopy Reveals Hydrogen Bond Dynamics of Aromatic Nitriles. Chem. Phys. Lett. 2009; 469:325–330. [PubMed: 20622983]
29. Maekawa H, Ge N-H. Picosecond Rotational Interconversion Adjacent to a C═O Bond Studied by Two-Dimensional Infrared Spectroscopy. J. Phys. Chem. B. 2012; 116:11292–11301. [PubMed: 22931373]
30. Lee K-K, Park K-H, Joo C, Kwon H-J, Han H, Ha J-H, Park S, Cho M. Ultrafast Internal Rotational Dynamics of the Azido Group in (4s)-Azidoproline: Chemical Exchange 2D IR Spectroscopic Investigations. Chem. Phys. 2012; 396:23–29.
31. Thielges MC, Fayer MD. Protein Dynamics Studied with Ultrafast Two-Dimensional Infrared Vibrational Echo Spectroscopy. Acc. Chem. Res. 2012; 45:1866–1874. [PubMed: 22433178]
32. Kuroda DG, Bauman JD, Challa JR, Patel D, Troxler T, Das K, Arnold E, Hochstrasser RM. Snapshot of the Equilibrium Dynamics of a Drug Bound to Hiv-1 Reverse Transcriptase. Nature Chem. 2013; 5:1755–4330.
33. Middleton CT, Marek P, Cao P, Chiu C-c, Singh S, Woys AM, de Pablo JJ, Raleigh DP, Zanni MT. Two-Dimensional Infrared Spectroscopy Reveals the Complex Behaviour of an Amyloid Fibril Inhibitor. Nature Chem. 2012; 4:355–360. [PubMed: 22522254]
34. Vorobyev DY, Kuo C-H, Chen J-X, Kuroda DG, Scott JN, Vanderkooi JM, Hochstrasser RM. Ultrafast Vibrational Spectroscopy of a Degenerate Mode of Guanidinium Chloride. J. Phys. Chem. B. 2009; 113:15382–15391. [PubMed: 19905022]

35. Vorobyev DY, Kuo C-H, Kuroda DG, Scott JN, Vanderkooi JM, Hochstrasser RM. Water-Induced Relaxation of a Degenerate Vibration of Guanidinium Using 2D IR Echo Spectroscopy. J. Phys. Chem. B. 2010; 114:2944–2953. [PubMed: 20143800]
36. Kuroda DG, Singh PK, Hochstrasser RM. Differential Hydration of Tricyanomethanide Observed by Time Resolved Vibrational Spectroscopy. J. Phys. Chem. B. 2012; 117:4354–4364. [PubMed: 22934602]
37. Kuroda, DG.; Hochstrasser, RM. Polarization Anisotropy Effects for Degenerate Vibrational Levels. In: Fayer, MD., editor. Ultrafast Infrared Vibrational Spectroscopy. Boca Raton: CRC Press; 2013.
38. Ghosh A, Tucker MJ, Hochstrasser RM. Identification of Arginine Residues in Peptides by 2D-IR Echo Spectroscopy. J. Phys. Chem. A. 2011; 115:9731–9738. [PubMed: 21539337]
39. Kuroda DG, Hochstrasser RM. Two-Dimensional Infrared Spectral Signature and Hydration of the Oxalate Dianion. J. Chem. Phys. 2011; 135:204502. [PubMed: 22128938]
40. Marszalek M, Fei Z, Zhu D-R, Scopelliti R, Dyson PJ, Zakeeruddin SM, Grätzel M. Application of Ionic Liquids Containing Tricyanomethanide [C(Cn)3]– or Tetracyanoborate [B(Cn)4]–Anions in Dye-Sensitized Solar Cells. Inorg. Chem. 2011; 50:11561–11567. [PubMed: 22026738]
41. Hipps KW, Aplin AT. The Tricyanomethanide Ion: An Infrared, Raman, and Tunneling Spectroscopy Study Including Isotopic Substitution. J. Phys. Chem. 1985; 89:5459–5464.
42. Weidinger D, Houchins C, Owrutsky JC. Vibrational Dynamics of Tricyanomethanide. Chem. Phys. Lett. 2012:525–526. 60–63.
43. Cho M, Yu J-Y, Joo T, Nagasawa Y, Passino SA, Fleming GR. The Integrated Photon Echo and Solvation Dynamics. J. Phys. Chem. 1996; 100:11944–11953.
44. Kwac K, Cho M. Molecular Dynamics Simulation Study of N-Methylacetamide in Water. II. Two-Dimensional Infrared Pump-Probe Spectra. J. Chem. Phys. 2003; 119:2256–2263.
45. Kwak K, Rosenfeld DE, Fayer MD. Taking Apart the Two-Dimensional Infrared Vibrational Echo Spectra: More Information and Elimination of Distortions. J. Chem. Phys. 2008; 128:204505–204510. [PubMed: 18513030]
46. Zanni MT, Ge N-H, Kim YS, Hochstrasser RM. Two-Dimensional IR Spectroscopy Can Be Designed to Eliminate the Diagonal Peaks and Expose Only the Crosspeaks Needed for Structure Determination. Proc. Nat. Acad. Sci. 2001; 98:11265–11270. [PubMed: 11562493]
47. Ge N-H, Zanni MT, Hochstrasser RM. Effects of Vibrational Frequency Correlations on Two-Dimensional Infrared Spectra. J. Phys. Chem. A. 2001; 106:962–972.
48. Hochstrasser RM. Two-Dimensional IR-Spectroscopy: Polarization Anisotropy Effects. Chem. Phys. 2001; 266:273–284.
49. Baiz CR, Kubarych KJ, Geva E. Molecular Theory and Simulation of Coherence Transfer in Metal Carbonyls and Its Signature on Multidimensional Infrared Spectra. J. Phys. Chem. B. 2011; 115:5322–5339. [PubMed: 21375310]

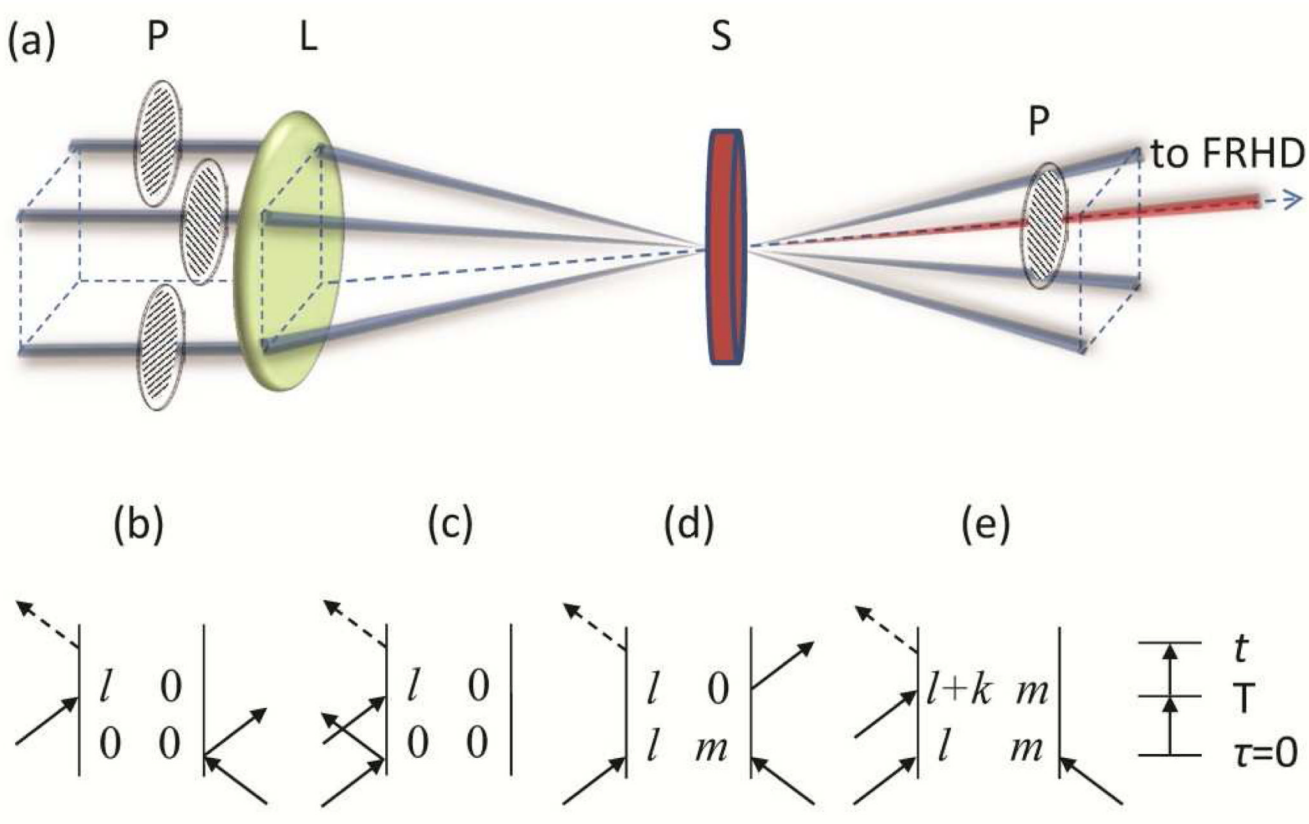

Figure 1.

(a) Schematic drawing of the polarization-selective BOXCARS setup. Gray beams represent incident mid-IR femtosecond laser pulses, red beam – vibrational photon echo emission, P – high-extinction wire-grid polarizers placed on each incident and emitted beam, L – focusing lens, S – sample cell, FRHD – frequency-resolved heterodyne detection. (b)–(e) Types of Liouville pathways involved in the heterodyned transient grating experiment. Here 0 represents the ground state and indices *l* and *m* are the fundamental modes of the molecule, and *l+k*, stands for the combination band if $l \neq k$ and for the overtone if *l=m=k*. Note that pathways in panels (b)–(c) involve interaction of the first pair of pulses with either *l* or *m* modes. The time sequence is shown to the right of the pathways.

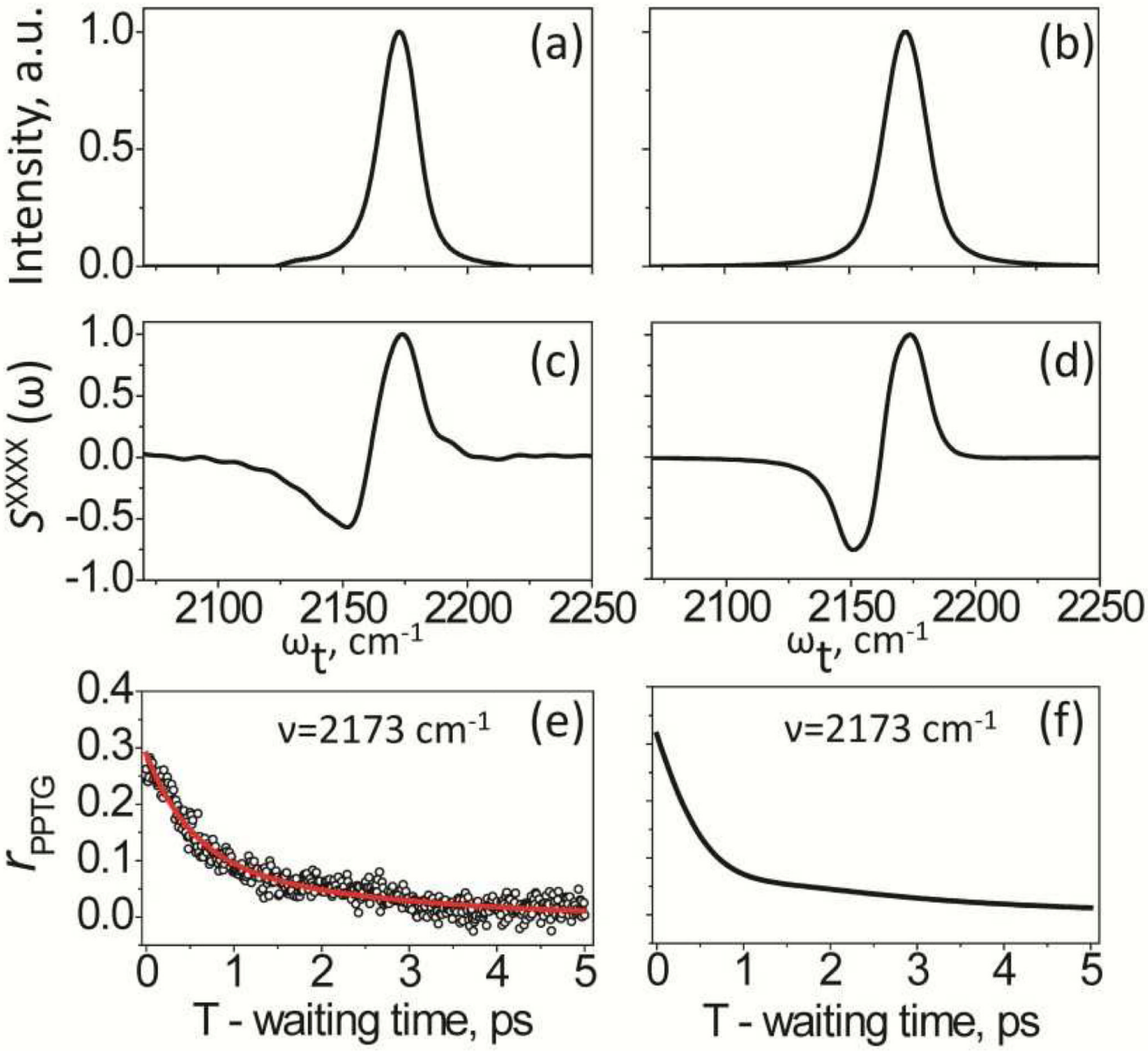

Figure 2.

Vibrational coherence relaxation of TCM in water: PPTG anisotropy. (a) Normalized linear infrared absorption spectrum with solvent background subtracted. (b) Numerically simulated linear absorption spectrum. (c) Real part of the experimental FRHTG signal $S^{XXXX}(\omega)$ at T=250 fs. The negative and positive peaks at 2152 and 2173 cm^{-1} correspond to the transient absorption and stimulated emission and ground state bleach signals, respectively. (d) Response functions-based simulation results of the FRHTG signal $S^{XXXX}(\omega)$, as in panel a. (e) PPTG anisotropy calculated at 2173 cm^{-1}. Open circles – experimental data, red line – fit to bi-exponential decay. (f) Simulated anisotropy waiting time dependence, with the population and coherence transfers included.

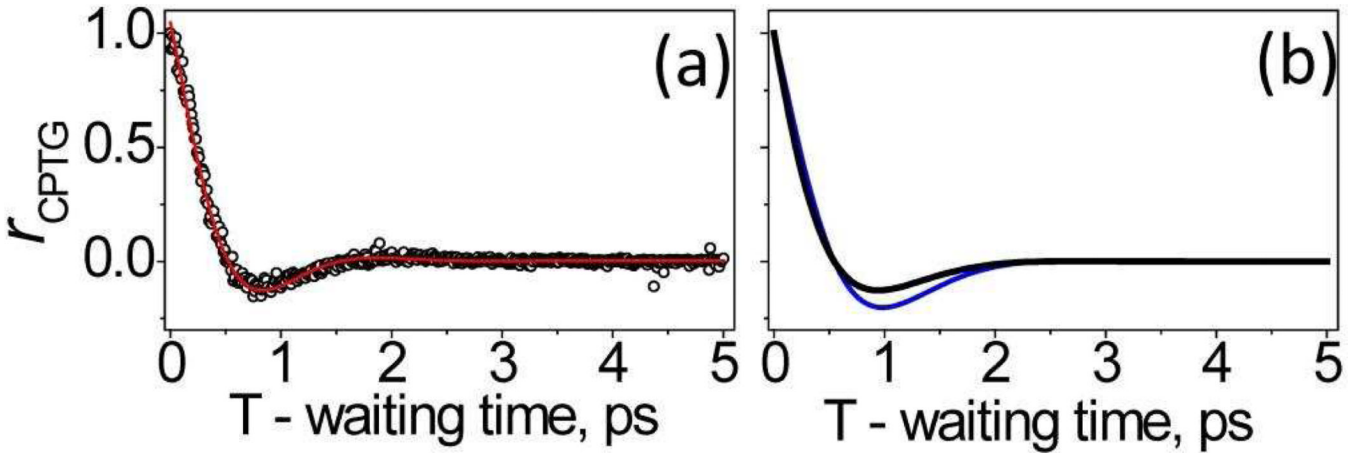

Figure 3.
Vibrational coherence relaxation of TCM in water: CPTG anisotropy. (a) Anisotropy calculated at 2173 cm^{-1}. The data is normalized to the value at T=0. Open circles – experimental data, red line – fit to equation (3). (b) Response functions-based simulation results of the two coupled vibrational modes with parameters from Table 1. Blue and black lines correspond to the cases where the contribution of the population and coherence transfer is omitted and included, respectively.

Table 1

Vibrational model parameters used for FRHTG signal simulations.

Parameters	TCM	
	mode 1	mode 2
ω, cm^{-1}	2167	2176
Δ, cm^{-1}	18[a]	
δ, cm^{-1}	15	
μ, arb. u.	1	1
T_1, ps	5	
$D \times 10^{10}$, s^{-1}	6.9	
k_{et}, ps^{-1}	0.7	
Δω, ps^{-1}	1.3[b]	
τ_C, ps	1.1	
f	0.5[b]	

[a] Δ is the anharmonicity of the vibrational modes.

[b] these parameters were chosen to best match experimental results.